Electron Number-Based Phase Diagram of $Pr_{1-x}LaCe_xCuO_{4-\delta}$ and Possible Absence of Disparity between Electron- and Hole-Doped Cuprate Phase Diagrams

Dongjoon Song,[1,*] Garam Han,[2,3] Wonshik Kyung,[2,3] Jeongjin Seo,[2,4] Soohyun Cho,[2,4] Beom Seo Kim,[2,3] Masashi Arita,[5] Kenya Shimada,[5] Hirofumi Namatame,[5] Masaki Taniguchi,[5] Y. Yoshida,[1] H. Eisaki,[1] Seung Ryong Park,[6] and C. Kim[2,3,†]

[1]*National Institute of Advanced Industrial Science and Technology, Tsukuba 305-8568, Japan*
[2]*Center for Correlated Electron Systems, Institute for Basic Science, Seoul 151-742, Republic of Korea*
[3]*Department of Physics and Astronomy, Seoul National University, Seoul 151-747, Republic of Korea*
[4]*Institute of Physics and Applied Physics, Yonsei University, Seoul 120-749, Republic of Korea*
[5]*Hiroshima Synchrotron Radiation Center, Hiroshima University, Higashi-Hiroshima, Hiroshima 739-0046, Japan*
[6]*Department of Physics, Incheon National University, Incheon 22012, Republic of Korea*

(Received 6 October 2016; published 28 March 2017)

We performed annealing and angle resolved photoemission spectroscopy studies on electron-doped cuprate $Pr_{1-x}LaCe_xCuO_{4-\delta}$ (PLCCO). It is found that the optimal annealing condition is dependent on the Ce content x. The electron number (n) is estimated from the experimentally obtained Fermi surface volume for $x = 0.10$, 0.15 and 0.18 samples. It clearly shows a significant and annealing dependent deviation from the nominal x. In addition, we observe that the pseudo-gap at hot spots is also closely correlated with n; the pseudogap gradually closes as n increases. We established a new phase diagram of PLCCO as a function of n. Different from the x-based one, the new phase diagram shows similar antiferromagnetic and superconducting phases to those of hole doped ones. Our results raise a possibility for absence of disparity between the phase diagrams of electron- and hole-doped cuprates

DOI: 10.1103/PhysRevLett.118.137001

In spite of the similar roles played by the charge carriers for cuprate high temperature superconductors, disparity between the phase diagrams of hole- and electron-doped materials appears to exist. While it is established that hole-doped cuprates have a clear phase separation between antiferromagnetic (AF) order and the superconducting (SC) state [1–3], it has been believed that the static AF order extends into the SC dome in the electron-doped case [4–6]. In addition, unlike the SC dome for the hole-doped case with an optimal doping around 15% [2,7,8], that for electron-doped materials shows a large variation [5,9–12]. Even the possibility for undoped superconductivity has recently been raised in thin film studies [13–15]. Still the exact phase diagram for electron-doped cuprates is unclear and under debate.

The controversy in the electron-doped cuprate phase diagram may be attributed to the conflicting experimental results associated with the annealing effect. Annealing, which is necessary in inducing the superconductivity, alters the oxygen content and significantly affects physical properties of the electron-doped materials [16]. For instance, despite sufficient Ce content and thus the doped electrons, as-grown materials exhibit AF order and insulating behaviors. However, upon proper annealing, the system turns into AF order free metallic state and the superconductivity emerges [17–21]. This annealing dependence in the physical properties has raised fundamental questions on the validity of the existing phase diagram constructed as a function of the Ce content.

An oxygen content (determined from the mass change during the annealing process) axis has been added to resolve the issues [18,20,21]. However, the mass change is not an exact measure of oxygen content in the sample. Moreover, the oxygen nonstoichiometry should affect the carrier concentration and the oxygen axis is thus coupled to the doping axis. Indeed, there are recent reports on angle resolved photoemission spectroscopy (ARPES) investigations of $Pr_{1.3}La_{0.6}Ce_{0.1}CuO_{4-\delta}$ single crystal and T'-La_2CuO_4 thin film which reveal that annealing and oxygen vacancy induce a sufficient change in the carrier density [22,23]. These results clearly indicate that the doping should be considered in conjunction with the annealing and oxygen nonstoichiometry and that the actual electron concentration n, instead of the Ce concentration x, should be used in building the phase diagram.

To find the true phase diagram and resolve the remaining issues, we have performed systematic ARPES experiments on $Pr_{1-x}LaCe_xCuO_{4-\delta}$ (PLCCO) single crystals ($x = 0.10$, 0.15, and 0.18) prepared under various annealing conditions. PLCCO is a suitable system because its T_c varies dramatically depending on the annealing condition [24,25] and the range for its controllable oxygen content is larger than other T' compounds [18]. We found that, different from the Ce based [5,26], the maximum T_c occurs at around $n = 0.15$ and that the deduced AF phase boundary does not extend into the SC dome. Therefore, the phase diagram we have determined looks very similar to that for the hole-doped cuprates.

High-quality PLCCO single crystals with $x = 0.10$, 0.15, and 0.18 were grown using the traveling-solvent floating-zone method. All the crystal rods were cleaved into small pieces and annealed in high-purity N_2 for 10–24 h at 920–930 °C. Subsequent air annealing was done on some of the samples at a temperature between 300 and 900 °C for 5–8 h. In naming the samples in Figs. 1–4, the first letter N refers to the initial annealing in N_2, and the second letter indicates the subsequent annealing either in air (A) or N_2 (N) with the number showing the post-annealing temperature. For the measured magnetic susceptibility in Fig. 1, the SC shielding volume fraction for the highest T_c sample of each Ce composition indicates the bulk superconductivity [5,20,26], and T_c is defined as the temperature corresponding to the 10% shielding signal. The ARPES experiments were performed at the beam line 5-4 of the Stanford Synchrotron Radiation Lightsource and beam line 9A of the Hiroshima Synchrotron Radiation Center. The experimental conditions for ARPES are the same as described in our earlier publication [25].

Figures 1(a)–1(c) show the magnetic susceptibility for $x = 0.10$, 0.15, and 0.18 samples, respectively, for different annealing conditions. A quick look at the data reveals that the T_c and SC shielding volume dramatically change with the annealing condition. For $x = 0.10$ in Fig. 1(a), oxygen reduction in the initial 920 °C N_2 annealing (N) induces superconductivity with $T_c \sim 25$ K, but subsequent N_2 annealing at a higher temperature lowers the T_c (NN930). On the other hand, post-air annealing at 300 °C (NA300) reduces the shielding fraction by half without a change in T_c. This likely means phase separation into normal and SC phase regions, for which the reason is presently unclear. Post-air annealing at 400 °C (NA400) leaves only a tiny fraction of the SC volume with an onset of $T_c \sim 11$ K. Although not plotted in Fig. 1(a), 500 °C post-air annealing completely eliminates the SC signal.

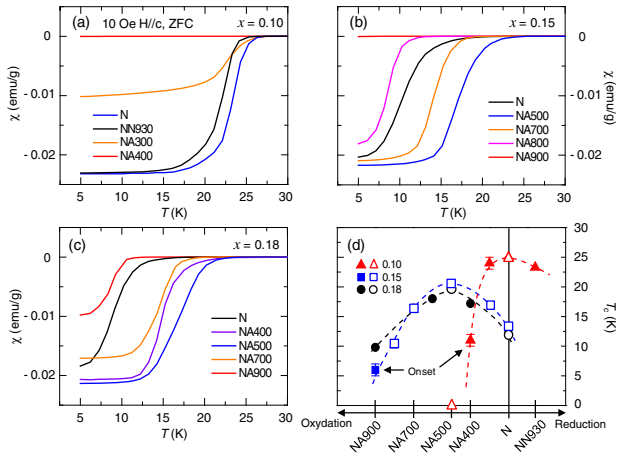

FIG. 1. Magnetic susceptibility of PLCCO for (a) $x = 0.10$, (b) $x = 0.15$, and (c) $x = 0.18$ measured under the zero-field cooled (ZFC) conditions. (d) T_c values for the data in panels (a)–(c) with respect to annealing conditions. Dotted lines are drawn to guide the eye. Open symbols indicate samples that were used in the ARPES study.

For $x = 0.15$ and 0.18 shown in Figs. 1(b) and 1(c), superconductivity is induced by the initial N_2 annealing (N) with a lower T_c compared to the case of $x = 0.10$. Surprisingly, subsequent post-air annealing at 400 °C (NA400) or 500 °C (NA500) increases T_c and the shielding volume, in a sharp contrast to the $x = 0.10$ case. On the other hand, increasing the post-air annealing temperature to above 600 °C results in a decrease in both T_c and the shielding fraction as seen in the data.

Figure 1(d) summarizes the relationship between the T_c and annealing conditions for the three values of x. As thermal energy accelerates the reaction and air (N_2) annealing is expected to increase (reduce) the oxygen content, we mark the higher-temperature post-air annealing side as "oxidation" while the opposite side is marked as "reduction." An important finding is that the annealing condition for the maximum T_c ($T_c^{\max}$) is different for $x = 0.10$ and $x = 0.15$ and 0.18. Specifically, the $T_c^{\max}$ region appears around N for $x = 0.10$ while it is around NA500 for $x = 0.15$ and 0.18. Another aspect to note is the dome-shaped variation of the T_c between oxidation and reduction, reminiscent of a doping-dependent SC dome. If this T_c dome with an optimal annealing condition is related to the charge carrier density, such an aspect should be reflected in the electronic structure.

The ARPES were carried out on the samples with the open symbol shown in Fig. 1(d), and Fermi surface (FS) maps of those samples are plotted in Figs. 2(a)–2(c). As is the case for other cuprates, the overall shape of the FS is like a circle centered at (π, π). Hot spots where the spectral weight is suppressed around $(2\pi/3, \pi/3)$ are observed in post-air annealed samples. For the x-dependent Fermiology with the annealing condition of NA500, the large and clear hot spots for $x = 0.10$ become weaker with increasing x, and the feature is fairly weak for $x = 0.18$. [See 10 NA500, 15 NA500, and 18 NA500 in Figs. 2(a), 2(b), and 2(c), respectively]. Similarly, a close inspection of the FS maps for differently annealed $x = 0.15$ in Fig. 2(b) reveals that the hot spots also depend on the annealing; as the air annealing temperature increases from 500 to 800 °C, the hot spot feature becomes stronger, which is analogous to what we see when x decreases. This suggests that increasing the post-air annealing temperature, which is more oxidation, reduces the charge carrier density of the system.

In order to see if the variation in Fermiology by annealing is indeed related to the charge carrier density, we assume a large circular FS centered at (π, π) and determined it from momentum distribution curve peak analysis as plotted in Figs. 2(d)–2(f). It should be pointed out that, although some of the FS maps (for example, 10 NA500 and 15 NA800) show fairly strong hot spot features, small but finite spectral weight at the Fermi level (E_F)

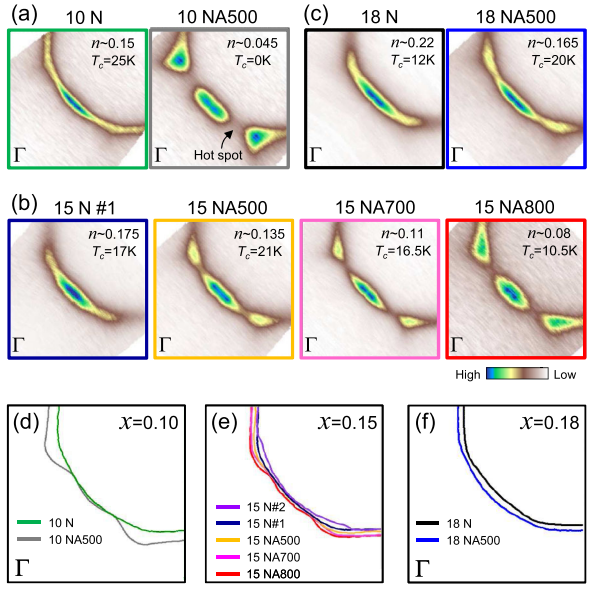

FIG. 2. (a)–(c) Fermi surface (FS) maps for various Ce concentrations and annealing conditions. Numbers 10, 15, and 18 in front of the annealing conditions indicate the Ce contents $x = 0.10$, 0.15, and 0.18, respectively. FS's are the spectral intensity within a ± 10 meV energy windows at the Fermi energy E_F. (d)–(f) FS's for $x = 0.10$, 0.15, and 0.18, respectively, obtained from the locus of the highest intensity in the FS maps. Both N#1 and N#2 were annealed in N_2 but with slightly different temperatures. FS's are color coded, matching the border color of panels (a)–(c).

enables us to do the peak analysis [27,28]. The resulting change in the enclosed area is easily seen in each panel, indicating significant annealing effects on the carrier density.

By using the Luttinger sum rule, we estimated the electron number n from the determined circular FSs which are considered to satisfy the Luttinger sum rule as demonstrated by Shubnikov–de Haas quantum oscillation studies [29,30]. We also calculated n based on two pocket FSs centered at $(\pi/2, \pi/2)$ and $(\pi, 0)$ [or $(0, \pi)$] for heavily under-n samples with strong hot spot features and found out that the difference is within the error bar. The estimated n's are plotted in Figs. 3(a)–3(c) along with T_c. We see that

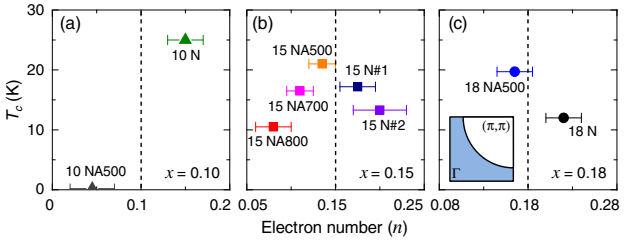

FIG. 3. (a)–(c) Electron number n dependence of T_c for $x = 0.10$, 0.15, and 0.18, respectively. The dashed lines indicate the nominal Ce content x. Shaded area of the FS schematic in (c) indicates the occupied states.

n for N samples is larger than x while NA samples have smaller n than x, which shows that reduction (oxidation) indeed injects electrons (holes) onto the CuO_2 planes. An important aspect of the data is that T_c becomes higher as n approaches the value about 0.15. This observation proposes that n plays a crucial role in determining T_c.

We now turn our attention to the pseudogap (PG) and AF phase. It has been well-established that the suppression of spectral weight near E_F resulting in PG at the hot spot is due to the (π, π) scattering from the AF order [31–33]. In this respect, we investigate the n dependence of PG at hot spots. In Figs. 4(a)–4(c), we plot the ARPES data along the FS contour for $n = 0.045$, 0.11, 0.22, respectively. For $n = 0.045$, strong spectral weight suppression or PG is evident between the nodal and the antinodal region as marked by a red-filled triangle. While the moderate suppression is observed near E_F even in the nodal region ($\theta \sim 0$), the band is still found to cross E_F. With increasing n, the weak intensity area shrinks, which is consistent with previous reports on doping dependence of PG [33–36].

Energy distribution curves (EDCs) at the hot spot are plotted in Fig. 4(d) for all the samples to examine the PG evolution quantitatively. The hot spot is defined as the point where Z, the ratio of spectral weight at E_F to the hump height around 100 meV, is the minimum. Overall, we see the larger spectral weight at E_F from the larger n sample. Accordingly, Z at the hot spot as a function of n shown in Fig. 4(e) reveals a monotonic increase in the in-gap spectral weight, starting from vanishing Z at $n = 0.045$. That is, PG gradually diminishes with n. This suggests that n is the key parameter not only for T_c but also for the AF phase.

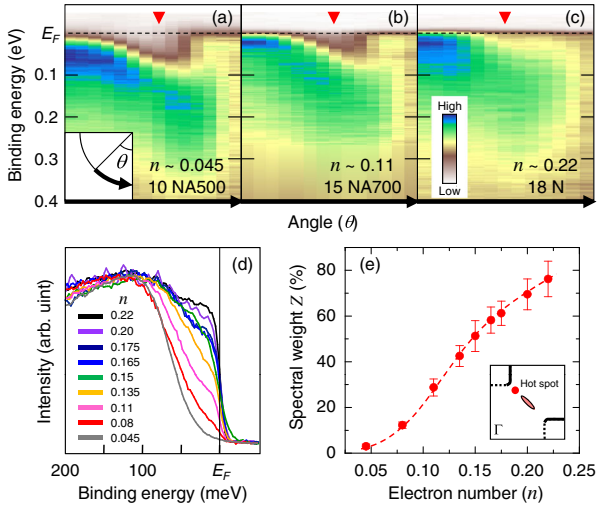

FIG. 4. ARPES data along the FS contour for n values of (a) 0.045, (b) 0.11, and (c) 0.22. Red-filled triangles in panels (a)–(c) indicate the locations of hot spots. The inset in (a) is a schematic of the FS contour along which data was taken. (d) EDCs at the hot spot from various samples. EDCs are color coded as in Fig. 2. (e) Spectral weight within 10 meV binding energy at the hot spot as a function of n.

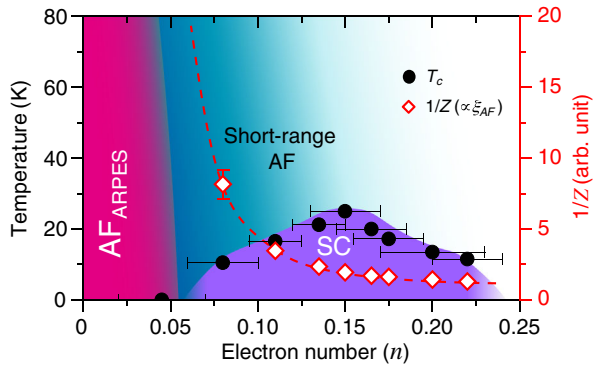

FIG. 5. New PLCCO phase diagram based on n. T_c values are indicated by black circles while red diamonds show the inverse of the hot spot spectral weight, $1/Z$. A long-range AF order (shaded in pink) and short-range and/or fluctuating AF order (shaded in light blue) are inferred from the ARPES data. $1/Z$ appears to diverge with decreasing n below ≈ 0.045 as indicated by the dotted red line.

We summarize the results in Figs. 3 and 4 as a T_c vs n phase diagram in Fig. 5. For Z at the hot spot, we plot $1/Z$ for the discussions to follow. First of all, we find that T_c data form a domelike shape or a SC dome (shaded in violet). The non-SC to SC state transition occurs between $n = 0.045$ and 0.08. Thereafter, T_c gradually increases to 25 K at $n = 0.15$, and then begins to decrease as n increases further. The shape of the resultant SC dome is thus obviously different from that based on x in which the maximum T_c occurs at $x \sim 0.10$ [5,26]. It is interesting to note that the SC dome spanning from 0.05 to 0.25 is rather similar to that of the hole-doped counterpart $La_{2-x}Sr_xCuO_4$ (LSCO) [7].

The n-dependent magnetism may also be inferred from the results. Previous studies have shown that the in-gap spectral weight at the hot spot is inversely proportional to the AF correlation length (ξ_{AF}), that is, $1/Z \propto \xi_{\mathrm{AF}}$ [33,34]. In this picture, the vanishing Z at $n = 0.045$ in Fig. 4(e) implies the presence of the long-range AF order. Whereas, increasing Z with n indicates that the long-range AF order at the experimental temperature $\sim$15 K is destroyed in between $n = 0.045$ and 0.08. As a result, the border of the AF phase may not overlap with the SC dome as depicted in Fig. 5. This observation is consistent with previous results from inelastic neutron scattering and low energy muon-spin rotation (μSR) measurements on $Nd_{2-x}Ce_xCuO_{4-\delta}$ (NCCO) single crystals and $La_{2-x}Ce_xCuO_{4-\delta}$ thin films, respectively [12,37]. Besides, the critical carrier concentration around 0.05 is similar to that of hole-doped cuprates [1,3]. Therefore, present results raise a possibility for absence of disparity between the phase diagrams of electron- and hole-doped cuprates. It would be desirable to verify it by a direct technique such as neutron scattering or μSR.

The possible absence of disparity in the phase diagram may have significant implications. There have been discussions on what causes the asymmetry between the phase diagrams of electron- and hole-doped cuprates, because it is expected that its origin could provide an essential clue to the SC mechanism. However, a rather identical phase diagram of PLCCO to that of, for example, LSCO as proposed here suggests that the character of the charge carrier may not play an essential role in the determination of the phase diagram. Indeed, despite the fact that the doped electron and hole reside at different sites (Cu $3d^{10}$ and Cu-O hybridized $3d^9\underline{L}$ states, respectively), an effective model, namely, the Zhang-Rice singlet that reduces the three band Hubbard model to the one band Hubbard model and then to the t-J model, assigns a $3d^8$ state to the hole, and thus leads to an electron-hole symmetry [16,38].

Meanwhile, the notion of a decisive role of the next-nearest neighbor hopping t' in stabilizing the AF phase has been raised in theoretical studies [39,40]. However, experimentally extracted t' does not show noticeable correlation with the robustness of AF order. For example, despite the more robust long-range AF order in NCCO than PLCCO, $-t'/t = 0.2 \pm 0.02$ obtained by applying a two-dimensional tight-binding model fitting to the FS of our PLCCO ($x = 0.15$) is quite similar to the reported value for NCCO ($x = 0.15$) [41]. One possibility is that the AF correlation depends not only on t' but also on the exchange coupling J. We note that the hump energy of $\sim$100 meV at the hot spot shown in Fig. 4(d) is smaller than that of NCCO of $\sim$150 meV. This indicates that J of PLCCO might be smaller than that of NCCO, since the size of PG is considered to be a measure of the effective J [34]. Previous reports consistently show that J in Pr_2CuO_4 is smaller than J in Nd_2CuO_4 [42]. On the other hand, we should mention that the n-based phase diagram needs to be obtained for NCCO to clearly resolve this issue.

For the n range above 0.045, n dependence of $1/Z$ in Fig. 5 shows how the short-range AF order vanishes with increasing electron doping. With the assumption of $1/Z \propto \xi_{\mathrm{AF}}$, ξ_{AF} decreases dramatically with the emergence of superconductivity as n increases in the under-n side, whereas it decreases rather moderately in the optimal- or over-n region. Consequently, ξ_{AF} in the under-n region is much longer compared to that in the optimal- and over-n regions. This short-range AF phase with a moderately long ξ_{AF} in the under-n region may explain why some measurements have shown overlap of AF and SC phases [4–6].

As a final note, there has been a recent report that argues for the absence of PG when no as-grown phase is left. The work was based on ARPES results from $Pr_{1.3}La_{0.6}Ce_{0.1}CuO_{4-\delta}$ ($\delta > 0$) that utilized the so-called "protect annealing" method [22]. In this regard, the normal N_2 annealing method used in our study may have left a tiny amount of the as-grown phase in the samples and the AF correlation may have been overestimated. However, we believe that such an effect is insignificant considering the

fact that the SC volume is close to 100%. In addition, various measurement techniques also have shown signatures of short-range or fluctuating AF order even for the protect annealed samples [43,44].

We acknowledge fruitful discussions with T. Tohyama and Y. K. Bang and helpful comments from S. Ishida, M. Horio, and A. Fujimori. This work was supported by the research program of Institute for Basic Science (Grant No. IBS-R009-G2) and JSPS KAKENHI (Grant No. 16H03854). D. S. was an international research fellow of JSPS. S. R. P. acknowledges support from the National Research Foundation of Korea (NRF) (Grant No. 2014R1A1A1002440). ARPES experiments were performed at SSRL operated by the DOE Office of BES (Proposal No. 4125) and HiSOR (Proposal No. 15-A-72).

*dj-son@aist.go.jp
†changyoung@snu.ac.kr

[1] H. Takagi, Y. Tokura, and S. Uchida, Physica C (Amsterdam) **162–164**, 1001 (1989).
[2] N. Doiron-Leyraud, C. Proust, D. LeBoeuf, J. Levallois, J.-B. Bonnemaison, R. Liang, D. A. Bonn, W. N. Hardy, and L. Taillefer, Nature (London) **447**, 565 (2007).
[3] B. Keimer, S. A. Kivelson, M. R. Norman, S. Uchida, and J. Zaanen, Nature (London) **518**, 179 (2015).
[4] P. K. Mang, O. P. Vajk, A. Arvanitaki, J. W. Lynn, and M. Greven, Phys. Rev. Lett. **93**, 027002 (2004).
[5] M. Fujita, T. Kubo, S. Kuroshima, T. Uefuji, K. Kawashima, K. Yamada, I. Watanabe, and K. Nagamine, Phys. Rev. B **67**, 014514 (2003).
[6] K. Jin, X. H. Zhang, P. Bach, and R. L. Greene, Phys. Rev. B **80**, 012501 (2009).
[7] H. Takagi, T. Ido, S. Ishibashi, M. Uota, S. Uchida, and Y. Tokura, Phys. Rev. B **40**, 2254 (1989).
[8] I. M. Vishik *et al.* Proc. Natl. Acad. Sci. U.S.A. **109**, 18332 (2012).
[9] H. Takagi, S. Uchida, and Y. Tokura, Phys. Rev. Lett. **62**, 1197 (1989).
[10] M. Brinkmann, T. Rex, H. Bach, and K. Westerholt, Phys. Rev. Lett. **74**, 4927 (1995).
[11] Y. Krockenberger, J. Kurian, A. Winkler, A. Tsukada, M. Naito, and L. Alff, Phys. Rev. B **77**, 060505(R) (2008).
[12] H. Saadaoui *et al.*, Nat. Commun. **6**, 6041 (2015).
[13] Y. Krockenberger, H. Irie, O. Matsumoto, K. Yamagami, M. Mitsuhashi, A. Tsukada, M. Naito, and H. Yamamoto, Sci. Rep. **3**, 2235 (2013).
[14] K. M. Kojima, Y. Krockenberger, I. Yamauchi, M. Miyazaki, M. Hiraishi, A. Koda, R. Kadono, R. Kumai, H. Yamamoto, A. Ikeda, and M. Naito, Phys. Rev. B **89**, 180508(R) (2014).
[15] G. Chanda, R. P. S. M. Lobo, E. Schachinger, J. Wosnitza, M. Naito, and A. V. Pronin, Phys. Rev. B **90**, 024503 (2014).
[16] N. P. Armitage, P. Fournier, and R. L. Greene, Rev. Mod. Phys. **82**, 2421 (2010).
[17] W. Jiang, J. L. Peng, Z. Y. Li, and R. L. Greene, Phys. Rev. B **47**, 8151 (1993).
[18] S. Kuroshima, M. Fujita, T. Uefuji, M. Matsuda, and K. Yamada, Physica C (Amsterdam) **392–396**, 216 (2003).
[19] P. Dai, H. J. Kang, H. A. Mook, M. Matsuura, J. W. Lynn, Y. Kurita, S. Komiya, and Y. Ando, Phys. Rev. B **71**, 100502 (R) (2005).
[20] H. J. Kang, P. Dai, H. A. Mook, D. N. Argyriou, V. Sikolenko, J. W. Lynn, Y. Kurita, S. Komiya, and Y. Ando, Phys. Rev. B **71**, 214512 (2005).
[21] S. D. Wilson, S. Li, P. Dai, W. Bao, J.-H. Chung, H. J. Kang, S.-H. Lee, S. Komiya, Y. Ando, and Q. Si, Phys. Rev. B **74**, 144514 (2006).
[22] M. Horio *et al.*, Nat. Commun. **7**, 10567 (2016).
[23] H. I. Wei, C. Adamo, E. A. Nowadnick, E. B. Lochocki, S. Chatterjee, J. P. Ruf, M. R. Beasley, D. G. Schlom, and K. M. Shen, Phys. Rev. Lett. **117**, 147002 (2016).
[24] Y.-L. Wang, Y. Huang, L. Shan, S. L. Li, P. Dai, C. Ren, and H.-H. Wen, Phys. Rev. B **80**, 094513 (2009).
[25] D. Song *et al.*, Phys. Rev. B **86**, 144520 (2012).
[26] M. Fujita, M. Matsuda, S.-H. Lee, M. Nakagawa, and K. Yamada, Phys. Rev. Lett. **101**, 107003 (2008).
[27] T. Yoshida *et al.*, Phys. Rev. B **74**, 224510 (2006).
[28] J. W. Harter, L. Maritato, D. E. Shai, E. J. Monkman, Y. Nie, D. G. Schlom, and K. M. Shen, Phys. Rev. Lett. **109**, 267001 (2012).
[29] M. V. Kartsovnik *et al.*, New J. Phys. **13**, 015001 (2011).
[30] T. Helm *et al.*, Phys. Rev. B **92**. 094501 (2015).
[31] N. P. Armitage *et al.*, Phys. Rev. Lett. **87**, 147003 (2001).
[32] H. Matsui, K. Terashima, T. Sato, T. Takahashi, S.-C. Wang, H.-B. Yang, H. Ding, T. Uefuji, and K. Yamada, Phys. Rev. Lett. **94**, 047005 (2005).
[33] S. R. Park *et al.*, Phys. Rev. B **87**, 174527 (2013).
[34] H. Matsui, T. Takahashi, T. Sato, K. Terashima, H. Ding, T. Uefuji, and K. Yamada, Phys. Rev. B **75**, 224514 (2007).
[35] Y. Onose, Y. Taguchi, K. Ishizaka, and Y. Tokura, Phys. Rev. Lett. **87**, 217001 (2001).
[36] A. Zimmers, J. M. Tomczak, R. P. S. M. Lobo, N. Bontemps, C. P. Hill, M. C. Barr, Y. Dagan, R. L. Greene, A. J. Millis, and C. C. Homes, Europhys. Lett. **70**, 225 (2005).
[37] E. M. Motoyama, G. Yu, I. M. Vishik, O. P. Vajk, P. K. Mang, and M. Greven, Nature (London) **445**, 186 (2007).
[38] F. C. Zhang and T. M. Rice, Phys. Rev. B **37**, 3759(R) (1988).
[39] T. Tohyama and S. Maekawa, Phys. Rev. B **64**, 212505 (2001).
[40] A. Singh, and H. Ghosh, Phys. Rev. B **65**, 134414 (2002).
[41] M. Ikeda, T. Yoshida, A. Fujimori, M. Kubota, K. Ono, H. Das, T. Saha-Dasgupta, K. Unozawa, Y. Kaga, T. Sasagawa, and H. Takagi, Phys. Rev. B **80**, 014510 (2009).
[42] Y. Ohta, T. Tohyama, and S. Maekawa, Phys. Rev. Lett. **66**, 1228 (1991).
[43] T. Adachi *et al.*, arXiv:1512.08095.
[44] M. Yamamoto, Y. Kohori, H. Fukazawa, A. Takahashi, T. Ohgi, T. Adachi, and Y. Koike, J. Phys. Soc. Jpn. **85**, 024708 (2016).